The atomistic mechanism of high temperature contact line advancement: results from molecular dynamics simulations

2009 J. Phys.: Condens. Matter 21 464135

(http://iopscience.iop.org/0953-8984/21/46/464135)

IOP PUBLISHING JOURNAL OF PHYSICS: CONDENSED MATTER

J. Phys.: Condens. Matter **21** (2009) 464135 (13pp) doi:10.1088/0953-8984/21/46/464135

The atomistic mechanism of high temperature contact line advancement: results from molecular dynamics simulations

Y Sun[1] and E B Webb III[2]

[1] Drexel University, Philadelphia, PA 19104, USA
[2] Sandia National Laboratories, Albuquerque, NM 87185, USA

E-mail: ysun@coe.drexel.edu and ebwebb@sandia.gov

Received 7 May 2009, in final form 1 September 2009
Published 29 October 2009
Online at stacks.iop.org/JPhysCM/21/464135

Abstract

Atomic scale phenomena driving contact line advancement during the wetting of a solid by a liquid are investigated via molecular dynamics simulations of Ag(l) drops spreading on Ni substrates. For the homologous temperature ∼5% above melting for Ag, essentially non-reactive wetting is observed with relatively high spreading velocity. Analyzing atomic positions with time, including computing flow fields, permits investigation of atomic scale transport mechanisms associated with advancement of the contact line. Delivery of material to the contact line occurs preferentially along the liquid/vapor interface. Ag(l) atoms transported along the liquid/vapor interface become new droplet edge material, effectively displacing existing edge material. Evidence is also shown of a prominent transport and flow mechanism more typically associated with the molecular kinetic theory of spreading: some portion of Ag(l) atoms move along the solid/liquid interface to eventually occupy the contact line region. Selected atomic trajectories are shown to illustrate atoms moving with the contact line, detaching and re-attaching at sites along the solid/liquid interface. However, this latter solid/liquid interface transport mechanism contributed a lower percentage of new material to the advancing contact line compared to the liquid/vapor interface transport mechanism. Features of the AgNi system that may contribute to the dominance of a liquid/vapor interface transport mechanism are highlighted, including a relatively low liquid/vapor surface tension.

1. Introduction

Wetting is the process of a liquid displacing another fluid (liquid or vapor) from a solid surface; it is driven by atomic phenomena local to the solid/liquid contact line. Good wetting is necessary to achieve extensive spreading, the macroscopic motion of a liquid phase along a solid surface. Wetting is important in many technological applications including materials joining, thin film coating, sintering, and corrosion processes [1, 2]. Self-cleaning surfaces of orchids, water gathering by desert insects, and other superhydrophobic surfaces are examples of wetting phenomena in nature [3]. Inert wetting occurs when the solid responds passively to wetting by the liquid; this is in contrast to reactive wetting, when a liquid reacts with the solid substrate on which it is spreading. Example behaviors observed between liquids and solids in reactive wetting scenarios include substrate dissolution and interfacial compound formation [4–6].

For non-reactive and reactive wetting, models have been advanced to connect wetting kinetics to relevant driving forces and dissipation mechanisms. The goal of these models is to establish expressions describing the rate at which a droplet's radius $R(t)$ changes in time t; such expressions are often of a power law form $R \sim t^{\alpha}$, where α is determined by the specific dissipation mechanism(s) assumed. Alternatively, expressions connecting the contact line velocity $v(t)$ to the contact angle $\theta(t)$ have been advanced. Such models can be distinguished in terms of which mechanisms are identified as being dominant in determining contact line kinetics. Non-reactive wetting kinetic models include those identifying liquid viscous forces

as the primary resistance to spreading [7, 8] as compared to those identifying molecular friction at the contact line as the dominant dissipation mechanism [9, 10]. Theories under the former description are hydrodynamic while those under the latter description are molecular kinetic. Models for describing reactive wetting kinetics typically invoke some aspect of the relevant reaction as being the dominant dissipation mechanism. One example assumes the rate of reaction at the solid/liquid interface dictates wetting kinetics (i.e. interface or reaction controlled) [6] while another assumes diffusion of reactants to the reaction zone limits spreading kinetics (diffusion controlled) [11]. Some reactive wetting systems show significant substrate dissolution into the spreading liquid and both experiments and models show the magnitude of dissolution may influence wetting kinetics [12, 13]. For some non-reactive and reactive wetting systems, a film of molecular thickness advances ahead of the main drop, acting as an additional dissipation mechanism [14–18]. Because wetting inherently involves the flow of liquid into a non-stationary, wedge shaped region, theory has been advanced that describes a rolling like, vortex motion in the liquid in the vicinity of the contact line [19]. Theoretical advancements and interpretation of experimental data would greatly benefit from accurate, atomic scale descriptions of the mechanisms responsible for advancement of a contact line. While it is clear that new solid/liquid and liquid/vapor interfaces are created (at the expense of solid/vapor interface), the atomic scale mechanisms responsible for this cannot be resolved with the existing experimental capabilities.

High temperature capillarity typically refers to wetting behavior in systems of metals and/or ceramics, where the melting point of constituent materials is well above room temperature. Such systems are often characterized as reactive wetting; for instance, reactions between a liquid and the wetted solid are exploited to create strong mechanical bonds in soldering and brazing processes for joining metals and ceramics. However, high temperature wetting may also occur without significant reaction, akin to what is observed for wetting of organic liquids at a much lower temperature (e.g. polydimethylsiloxane liquid on Si substrates) [20]. Understanding fundamental high temperature wetting processes permits the exploration of similarities and differences between relatively low melting point materials, such as polymers and short chain molecular liquids, and relatively high melting point materials, such as metals and ceramics. Understanding high temperature wetting at a phenomenological scale also has the potential for tremendous economic impact because of its relevance to a wide range of industries, including microelectronics, automotive, and aerospace. High temperatures challenge experiments to probe the fundamental processes of wetting; additional challenges emerge because experiments lack sufficient temporal and spatial resolution to thoroughly explore the atomic scale processes of wetting. Recent work by Saiz *et al* [20, 21] and by Yin *et al* [5] provide examples of the wealth of data and insight available from state of the art experimental techniques. Efforts such as these are invaluable to our understanding of high temperature wetting; nonetheless, models which resolve materials at the atomic scale, such as molecular dynamics (MD) simulations, have proven to be a useful counterpart to experiments for understanding high temperature wetting phenomena.

Numerical simulation techniques that resolve matter at the atomic scale provide detailed descriptions of processes driving wetting and spreading. Kinetics observed in simulations can be directly correlated with atomic phenomena underlying contact line advancement. This may permit enhanced interpretation of data obtained from experimental wetting studies and advance development of theoretical models describing contact line dynamics. In this paper, we briefly review the molecular dynamics (MD) simulation technique as a tool for investigating high temperature wetting and spreading. Results are then presented from MD simulations of Ag(l) spreading on Ni. In prior work, Moon *et al* used MD simulations to study this same system but for temperatures below the Ag melting point [17]. They observed the advancement of a precursor film with $R_f \sim t^{1/2}$. In accord with immiscibility illustrated in the experimental bulk binary Ag/Ni phase diagram, no reaction was observed between the spreading Ag and the underlying Ni substrate. Results are presented here for wetting at temperatures above the Ag melting point. The monoatomic nature of metallic liquids presents a straightforward case for examining wetting mechanisms at the atomic scale, compared perhaps to more complex molecular fluids where atomic scale transport is inherently a more concerted process. Because immiscibility exists in the Ag/Ni system, complications due to reactions are essentially removed. We emphasize this by presenting a detailed account of atomistic behavior near the contact line as a function of time. A picture emerges of the collective behavior driving advancement of a liquid across a solid surface. The remainder of the paper is organized as follows: in section 2, a brief review of MD as a simulation technique for studying high temperature capillarity is presented. The computational procedure used herein is discussed in section 3, results are presented and discussed in section 4, and conclusions are summarized in section 5.

2. MD simulations of high temperature capillarity

The molecular dynamics (MD) technique is widely used to model material behavior at the atomic scale. It is straightforward in implementation: a mathematical connection is formulated to describe the energy of a system as a function of the constituent atomic coordinates. The derivative of system energy with respect to an atom's position permits calculation of the force on the atom. Given this methodology, the force on every atom in a given system is determined and Newton's equations of motion are solved to integrate the atomic positions forward in time by some small increment (typically ∼1 fs). This process is repeated to obtain a time and space trajectory of the atomic system; in this fashion, system properties can be calculated including structural features, thermodynamic quantities, and transport coefficients [22]. MD simulations can be run in equilibrium system ensembles; alternatively, non-equilibrium ensembles can be adopted. In the latter case, a driving force is applied to the system and

transient and steady state behavior is observed to obtain non-equilibrium system properties (and, perhaps, extrapolation to equilibrium properties). For simulations of liquids wetting solids, the driving force is capillary and is typically achieved by constructing the simulation starting state so that the constituent materials are out of equilibrium. Examples include models of sessile drop geometry, which assume a simulation starting state that is a spherical or cylindrical drop in contact with a solid substrate such that the initial contact angle is 180°. The atomic trajectory in such models permits, for instance, calculation of the time dependent contact line velocity $v(t)$, contact angle $\theta(t)$, and droplet radius $R(t)$.

The application of atomic scale simulations (e.g., MD) to study high temperature wetting was reviewed previously [23]; more recently, the MD method as applied to wetting of simple liquids was reviewed [24]. A brief summary of some results pertinent to high temperature wetting is given here to motivate the current work. As alluded to already, binary bulk phase behavior sometimes provides an indication of reactivity during wetting: the Ag/Cu system is eutectic and experiments observe significant substrate dissolution when Ag(l) wets Cu [4]. Similarly, models of wetting in this system revealed dissolutive spreading with kinetics that were well described by $R \sim t^{1/2}$ [13]. Another example is Pb/Cu, a system that exhibits bulk immiscibility, even in the liquid state. Experiments for this system exhibit no substrate dissolution and this, too, is found in simulations for Pb(l) drops on Cu [18, 25–27]. However, this system also shows that binary phase behavior is not sufficient to fully understand wetting phenomena. Although the Pb/Cu system is bulk immiscible, surface alloy phases have been observed for Pb on Cu surfaces in both experiment and simulation [18, 27–29]. In simulations of wetting in this system, formation of a surface alloy phase was demonstrated to limit wetting kinetics [18].

Simulations have also been combined with thermodynamic calculations to assess the magnitude of influence reactivity has on wetting kinetics. Specifically, a eutectic, dissolutive wetting system (Cu(l)/Ni) was simulated in a pore infiltration geometry [30]. Theory predicts that pore infiltration follows $L \sim t^{1/2}$ [31] and simulations for Cu(l) infiltrating Ni in [30] agreed with theory for temperatures at which dissolution was not aggressive. However, for pronounced dissolution, simulation results for infiltration kinetics deviated from theory. Thermodynamic calculations were used to present a modified form of infiltration theory, accounting for the free energy of dissolution. Reference [30] shows the modified form must be used when the dissolution free energy is comparable (or larger) in magnitude than the capillary (surface) energy.

A powerful aspect of MD is its resolution, spatially and temporally. Herein, this resolution is used to explore a high temperature system but focus is placed on an example for which reactions play a negligible role during wetting. In this fashion, atomic scale behavior can be explored to answer mechanistic questions such as, during formation of a new solid/liquid (and liquid/vapor) interface, how is material delivered to the interface, that is, to the contact line? Also, what atomistic mechanisms in close proximity to the contact line act to deliver material from farther away in the 'bulk' of the drop? Answering such questions can be complicated by a lack of sufficient statistics unless a relatively large liquid drop is simulated. Atomic scale resolution places limits on this but droplets modeled herein are large enough that a consistent description of observed mechanisms is possible. Simulations permit a very detailed view of fundamental wetting mechanisms and results presented are used to provide further interpretation into molecular scale wetting theory.

3. Simulation procedure

Interactions in our MD simulations were described using interatomic potentials formulated within the embedded atom method (EAM) [32]. The EAM employs a multibody interaction to describe bonding wherein the total energy for N atoms is

$$E = \sum_{i=1}^{N} \left[F_i(\rho_i) + \tfrac{1}{2} \sum_{j \neq i} \phi_{ij}(R) \right]. \quad (1)$$

Here $F_i(\rho_i)$ is the energy associated with embedding atom i into an electron density ρ_i, $\rho_i = \sum_{j \neq i} \rho_j^a(R)$, where $\rho_j^a(R)$ is the spherically symmetric electron density contributed by atom j, a distance R from i, $\phi_{ij}(R)$ is a pair potential between atoms i and j. The EAM has been widely used in performing atomistic simulations of metals and the EAM potentials for pure Ag, pure Ni, and AgNi alloy used here were developed by Foiles *et al* [33]. For fitting the interaction between Ag and Ni atoms, a positive single substitutional impurity heat of solution was required, in accord with immiscibility exhibited in the bulk binary phase diagram [34]. Recent calculations of Ag melting point using this potential parameterization gave $T_{\mathrm{m}}^{\mathrm{Ag}} = 1144$ K, which can be compared to the experimental $T_{\mathrm{m}}^{\mathrm{Ag}} = 1235$ K [35]. Wetting was modeled at $T = 1200$ K, ~5% greater than T_{m} predicted by this model for Ag, and also at $T = 1500$ K, which is still well below the model prediction for the Ni melting point, $T_{\mathrm{m}}^{\mathrm{Ni}} = 1740$ K (determined by free energy calculations [36]). The wetting geometry modeled is a cylindrical drop of Ag(l) in contact with Ni, where the cylinder axis is along y and one-dimensional spreading occurs along x. The free surface direction for Ni substrates is along z. Periodic boundary conditions are enforced in x and y but not in z; as such, this models an infinite line of liquid spreading on a substrate. For brevity, the liquid cylinder is referred to as a drop herein.

The Ni FCC crystals were constructed with the [111] or [100] direction oriented along the z axis of the simulation cell. The zero pressure lattice constant a_0 for each temperature T of interest was determined from separate simulations in constant number, pressure, and temperature NPT equilibrium ensembles with $N = 4000$ atoms. The dimensions of Ni substrate slabs for wetting simulations equaled the overall cell dimensions in x and y; they were $L_x = 220.8$ nm and $L_y = 2.5$ nm. The thickness of the Ni substrates in the free surface direction z was 5.6 nm. Since the liquid drop was only placed on one surface, atoms at the other surface in z were held frozen for subsequent calculations; the thickness of the frozen region was $3a_0$. The remaining atoms in the substrate were allowed to relax according to MD equations of motion and each substrate

system was equilibrated at constant T using a Nose–Hoover thermostat.

Separately, Ag liquids were equilibrated at $T = 1200$ and 1500 K in *NPT* ensemble simulations; however, only the x and z dimensions of the liquid slabs were permitted to relax according to the constant pressure algorithm. The y dimension of the liquid slabs was held constant at a value determined by the y dimension of the corresponding Ni solid slabs. Cylindrical slugs with desired initial radii, $R_0 = 25$ nm, were then cut out of these systems and equilibrated in free space by removing periodic boundary conditions in x and z but maintaining them in y. The equilibrated cylinder was then placed in a simulation box just above the equilibrated Ni surface with an initial separation distance corresponding to the minimum energy separation distance in the Ag–Ni interaction potential. After joining the liquid and solid, all subsequent calculations were done in a microcanonical (*NVE*) integration for the entire Ag(l) drop and the top $3a_0$ thick layer of the Ni substrate in z; for the remainder of the dynamic system, integration within a canonical (*NVT*) ensemble was performed. This was done to model isothermal wetting while ensuring that the thermostat algorithm did not influence hydrodynamics in the liquid droplet. Calculations were performed with the large-scale parallel code LAMMPS [37]. All simulations used a 1 fs time step.

To determine the time dependent radius $R(t)$ of the spreading drop and the contact angle $\theta(t)$, slabs or layers were defined in the simulation cell parallel to the Ni surface with a thickness in z equal to the Ni planar spacing ($\sim$0.2 nm). The layer containing the surface Ni plane at $t = 0$ was designated as $l = -1$ and layers above the Ni surface were designated $l = 1, 2, 3, \ldots$. Within each layer at a given t, the density of drop atoms was calculated as a function of distance from the layer's center of mass. Density data were integrated until 98% of drop atoms in the layer were accounted for; the distance at which this occurred was $R(t)$ for the layer l. The criterion of less than 100% was used to avoid erroneous data generated by single Ag atoms breaking away from the drop and diffusing across the Ni surface; slight changes in this criterion do not effect the conclusions obtained from simulations [13]. By performing this analysis in different layers, we obtained $R(t)$ as a function of height, h, above the Ni surface. The slope of a linear fit to h versus $R(t)$ data between two and six layers above the substrate surface gave $\theta(t)$. This method permits us to skip the precursor film layer and directly extract the contact angle exhibited within $\sim$1.5 nm of the substrate surface. In a prior publication, this method was compared to fitting the entire droplet surface with a circular section profile and it was shown that the method used herein gave a more accurate depiction of the droplet shape near the contact line [13]. Number density profiles along the z axis of the simulation cell were calculated to probe the Ag–Ni interfacial region. The analysis was restricted to atoms whose distance from the initial point of contact between drop and substrate in x was less than 5 nm. Velocity vector maps (flow fields) were generated by collapsing all atomic coordinates into the xz plane, on which a square analysis grid was established with grid elements 0.5 nm $\times$ 0.5 nm. The average (x, z) position of all atoms in each grid element was calculated at the beginning and end of a time interval; this permitted calculation of the average displacement, and therefore velocity, for material in each grid during that time span. To explore the correlation between contact line velocity and $\cos\theta$, velocities and contact angles were averaged using ten instantaneous values obtained every 4 ps to reduce scatter in the data.

4. Results and discussion

MD simulations of Ag(l) drops wetting Ni(100) and Ni(111) at $T = 1500$ K exhibited relatively significant substrate dissolution into the spreading drop. Similar to what has been observed previously in dissolutive wetting simulations of Ag(l) on Cu [13], drop radius kinetics from present results for Ag(l) on Ni at $T = 1500$ K were well described by $R \sim t^{1/2}$. Also similar to prior results: no precursor foot was observed during dissolutive wetting, a low steady state advancing contact angle was obtained $\theta_{SS} \lesssim 10°$, and negligible difference was found for wetting Ni(100) versus Ni(111). Given the positive heat of mixing predicted by the AgNi force field employed [33] along with the relative immiscibility exhibited by the MD simulation [17], dissolutive behavior is somewhat surprising. However, these results are for a fairly high homologous temperature, $T^* = 1.31$. As an illustration of the relative immiscibility in the system modeled here, the dissolution rate in present simulations for Ag(l) on Ni at $T^* = 1.31$ is lower than what was observed for the eutectic system of Ag(l) on Cu at $T^* = 1.05$. It is important to highlight that little emphasis was placed on optimizing the description of binary AgNi behavior during the initial parameter development for the interatomic force field employed here [33]. As such, comparing the degree of dissolution between the model and experiment for this T remains an outstanding validation exercise, beyond the scope of this paper. The goal herein is to elucidate wetting mechanisms in a metallic system that shows negligible reactivity during spreading. As presented in greater detail below, results at $T = 1200$ K demonstrate that substrate dissolution is dramatically reduced at this lower T. As such, focus throughout the remainder of the paper will be on the results from simulations for $T = 1200$ K.

Figure 1 shows simulation snapshots of a cylindrical Ag(l) drop wetting a Ni(100) surface at $T = 1200$ K. Darker spheres representing Ni atoms can be seen in the Ag(l) indicative that some dissolution is occurring. However, the degree or rate of dissolution is much lower at $T = 1200$ K compared to $T = 1500$ K. This is further illustrated in figure 2 where density profiles through the solid/liquid interface are shown for both temperatures after roughly 5 ns of simulation time. Data for figure 2 were obtained only from atoms with -5 nm $< x <$ 5 nm; thus, this region of the solid surface was covered by the liquid droplet in less than 0.1 ns of simulation time. The peaks in the solid curve to the left of each plot show the crystalline planes in Ni and the dotted curve shows data for Ag(l). Data in figure 2 demonstrate significantly less substrate dissolution occurs at $T = 1200$ K compared to $T = 1500$ K: in the former the solid/liquid interface has advanced 0.5 nm into the substrate while in the latter it is about five times that. Adding up Ag and

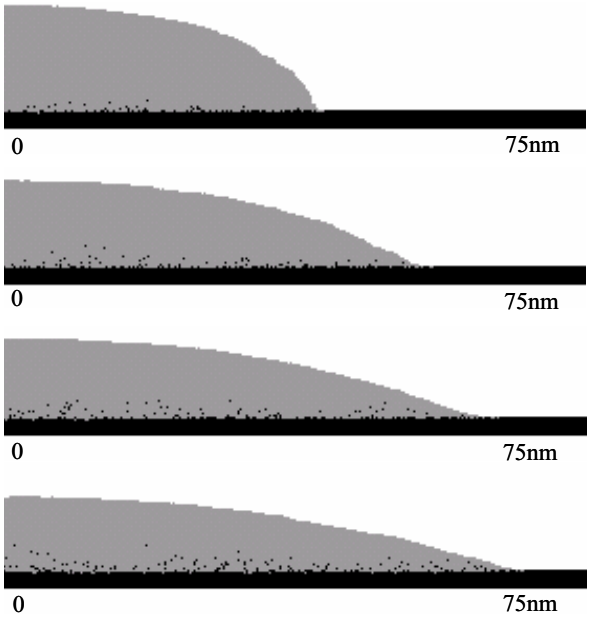

Figure 1. Cross-section snapshots of a cylindrical Ag(l) drop on Ni(100) at $T = 1200$ K. Images from top to bottom are shown for $t = 1$, 2, 3, and 4 ns; gray shows Ag and black shows Ni.

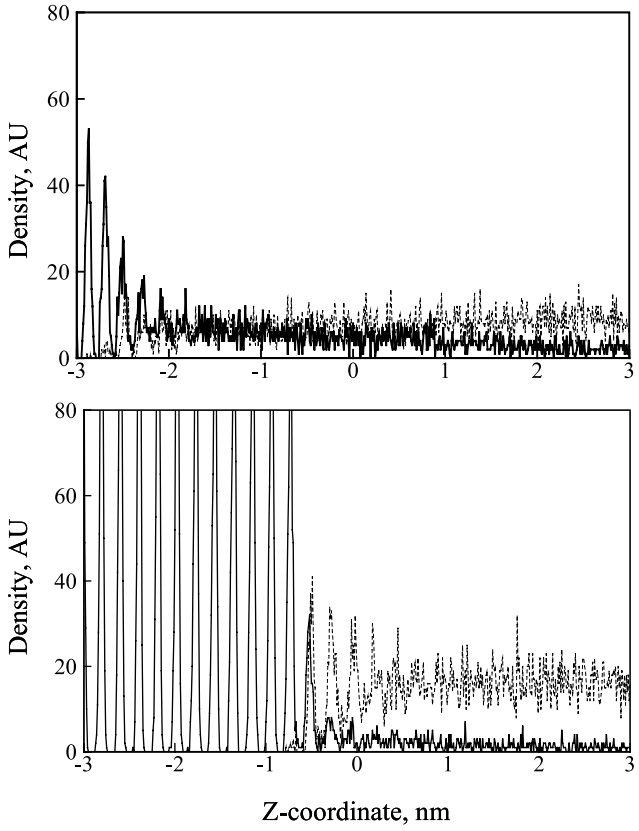

Figure 2. Density profiles of Ni (solid) and Ag (dotted) for wetting of a Ag(l) cylindrical drop on Ni(100) at $T = 1500$ K (top) and $T = 1200$ K (bottom). The original solid–liquid interface is located at $z = 0$.

Ni densities at each location in z, the total liquid densities are similar for both temperatures (i.e., the dependence of liquid density on temperature is negligible). However, Ag densities are different between two panes of figure 2 due to different degrees of dissolution at each temperature. Data such as those in figures 1 and 2 for Ag(l) on Ni(100) changed very little when compared to similar data for Ag(l) on Ni(111). At both T studied herein, minimal dependence of wetting behavior upon substrate crystal surface termination was found. As such, results hereafter are presented only for Ni(100).

Kinetics of a Ag(l) cylindrical drop wetting Ni(100) at $T = 1200$ K are presented in figure 3; data are shown for (a) $R^2(t)$ and (b) $\theta(t)$. In the first frame, data are shown for the drop radius in three analysis layers above the initial solid/liquid interface. Two regimes are apparent in $R^2(t)$: an earlier, relatively rapid regime ($t \lesssim 2$ ns) and a later, slower regime. While the later regime is relatively slower than the earlier regime, it is of note that droplet velocity throughout the simulation was over 1 m s^{-1}. Compared to many high temperature experiments in a sessile drop geometry, this is a high velocity spreading system. The reasons for this are partly that the capillary driving forces are high (i.e. the Ag(l) liquid/vapor surface tension is significantly lower than the Ni solid surface free energy). Also, the substrate surface over which the droplet spreads in our simulations is a single crystal without steps or features of any kind. Essentially, the Ag(l) spreads across a perfect crystal surface. While this is idealized relative to experiments and applications, it is still of use to consider atomic scale behavior in this ideal spreading scenario as it provides the most fundamental description of associated phenomena. Nonetheless, this feature likely contributes somewhat to the high spreading velocities observed. During the initial, relatively rapid spreading regime ($t \lesssim 2$ ns), $R^2(t)$ data for all three layers exhibit linearity, consistent with $R(t) \sim t^{1/2}$. Kinetics in the early stage are more rapid because the system is far out of capillary equilibrium so the corresponding driving forces are large. Saiz *et al* described this regime as an inertial one where the droplet does not exhibit constant curvature, leading to additional driving forces for spreading [20]. As a result, material is rapidly transported across the surface and $t^{1/2}$ kinetics are exhibited. While the slope of $R^2(t)$ data has units akin to a surface diffusion constant, spreading is a driven phenomenon so the magnitude of the slope for $R^2(t)$ data is different than the magnitude of surface diffusivity.

Contact angle data in figure 3(b) show $\theta(t)$ decreases very rapidly from the initial value of 180° to well under 90° in less than 1 ns. Figure 3 also shows that the transition to the later, slower wetting regime corresponds to a transition to a wedge shape contact line geometry with $\theta \lesssim 40°$. The capillary driving force decreases with contact angle; numerically, kinetic theories of wetting typically draw direct correlation between the capillary driving force and the negative of $\cos(\theta)$. In such cases—in line with physical intuition—the driving force is at a maximum when $\theta = 180°$, decreases rapidly as θ drops through 90°, and continues to decrease—but at a diminishing rate—as θ approaches its equilibrium value. For the present system for $\theta \lesssim 40°$, evidence suggests the capillary driving force has decreased dramatically from the initial state; this is

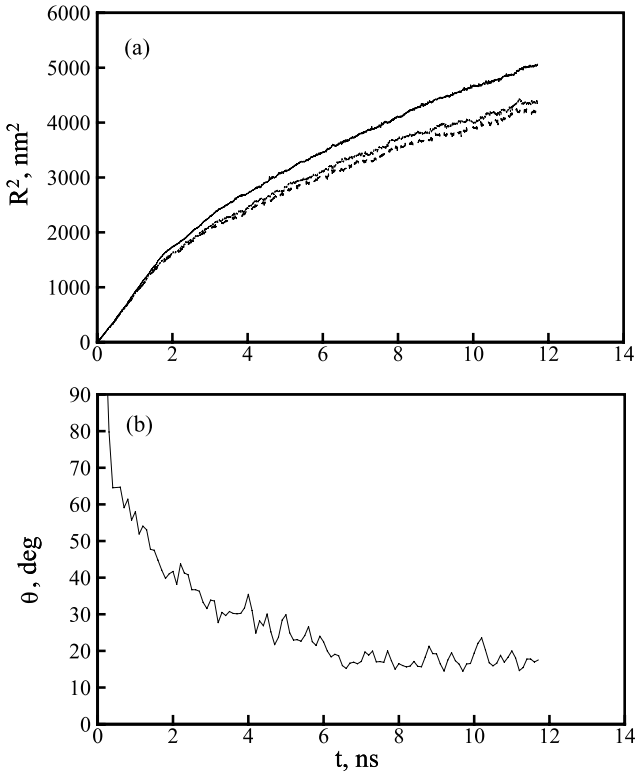

Figure 3. Kinetic data for Ag(l) wetting Ni(100) at $T = 1200$ K; (a) shows $R^2(t)$ for layers $l = 1$, 2, and 3, and (b) shows $\theta(t)$.

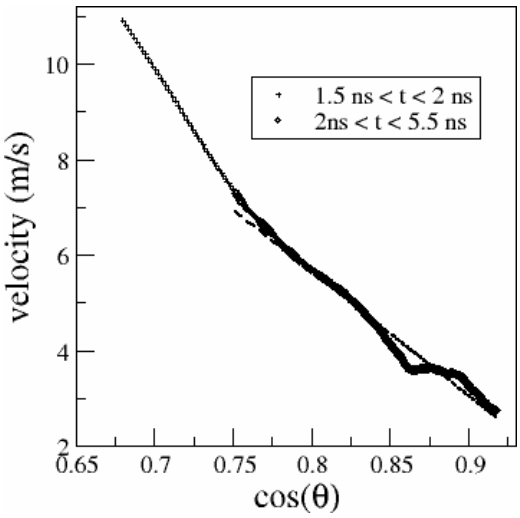

Figure 4. Drop spreading velocity versus $\cos\theta$ for a cylindrical Ag(l) drop on Ni(100) at $T = 1200$ K for $t = 1.5$–5.5 ns. Symbols distinguish between data for $t < 2$ and $t > 2$ ns; a dashed line shows the best fit to data for 2 ns $< t <$ 5.5 ns.

partly due to the droplet having adopted a constant curvature shape. As contact angle decreases below 40°, the wedge forming the edge of the drop narrows and transport of liquid to the contact line occurs through an effectively narrower path. In such a geometry, resistances due to viscous and/or interface forces are expected to become more pronounced. Correspondingly, a slower regime of wetting kinetics emerges.

During the slower spreading regime, figure 3(a) shows that data describing $R(t)$ in different layers above the solid/liquid interface become easier to distinguish. Indeed, the curve for $R(t)$ from layer 1 increasingly separates from curves for layers 2 and 3. The first layer curve is used to characterize precursor film kinetics while curves for data from layers 2 and 3 reflect kinetics of the main drop. Thus, separation of layer 1 data from data for layers 2 and 3 indicates the emergence of a precursor film, spreading ahead of the main drop. This is similar to what was observed in simulations below melting for this system [17]. Recall from the discussion above, though, that no precursor foot was observed for $T = 1500$ K. This is evidence that, above some T, kinetics of the main droplet become sufficiently rapid that the edge of the drop moves across the substrate surface at the same rate as that at which the precursor film advances. For layer 1 data, illustrative of precursor film advancement, $R \sim t^{1/2}$ kinetics are expected and fairly linear behavior is exhibited by that curve in figure 3(a), particularly once the film becomes separated from the main drop by a few nm ($t \gtrsim 8$ ns). Note this is also when the contact angle of the drop has reached a steady state advancing value, and oscillates around 18°. Data for the main droplet layers 2 and 3 exhibit negative curvature throughout the slower spreading regime, indicative of $R \sim t^{\alpha}$, with $\alpha < 1/2$. However, deviation from linearity is not significant, particularly for $t \gtrsim 8$ ns. Results presented suggest that this system exhibits kinetics similar to systems described previously as 'rapid spreading liquids' [38] and also similar to the non-reactive metals studied in [20]. Small deviation from $t^{1/2}$ behavior exhibited in figure 3(a) may be a result of dissipation due to precursor film advancement (note, precursor films were not observed in [20]). In addition, other dissipation mechanisms may be emerging.

It is clear from figures 1 and 2, that this is not a reactive wetting system. For the cylindrical droplet geometry adopted here, existing theories of inert wetting kinetics that predict power law behavior $R \sim t^{\alpha}$, where $\alpha < 1/2$ include molecular kinetic controlled wetting ($\alpha = 1/5$) and hydrodynamic controlled wetting ($\alpha = 1/7$) [39]. Because drop size is nanometer scale, interface related dissipation mechanisms are expected to be pronounced; however, fast spreading velocities increase the influence of hydrodynamic dissipation. Figure 4 explores this further by comparing the droplet spreading velocity v to $\cos(\theta)$. Note, data are included for 1.5 ns $< t <$ 5.5 ns; for $t \gtrsim 6$ ns, θ and v become roughly constant (deviations about average values are approximately 15% for θ and v in this time regime). Furthermore, data for $t < 2$ ns (i.e. the fast spreading regime) are distinguished from data for $t > 2$ ns, where slower spreading kinetics are observed in $R(t)$ data. As presented in [20], after simplifications appropriate to high temperature spreading of metals are made, the expression from molecular kinetic theory connecting droplet velocity to contact angle gives $v \sim \frac{\gamma_{LV}}{\zeta}\cos(\theta)$, where γ_{LV} is liquid/vapor surface tension (400 dyn cm^{-1} for the model used here [40]), and ζ is a friction term. Blake *et al* [9, 41] assumed contact line advancement was controlled by displacements of atoms from one adsorption site at the solid/liquid interface to another. In molecular kinetic theory, ζ represents friction between the solid and liquid. For results in figure 4, it is interesting to

note the very robust linear relation between v and $\cos(\theta)$ for data from $t < 2$ ns. For the remaining data, linearity is less pronounced; however, assuming linear dependence for later time is still reasonable as exhibited by the linear fit to data in figure 4 for $t > 2$ ns. From the slope obtained and γ_{LV} given above, $\zeta = 0.015$ Pa s. This is roughly two orders of magnitude less than friction terms obtained for Ag(l) on Mo in [20]. This is evidence that molecular kinetic dissipation mechanisms are relatively small in the present system. This does not necessarily mean that the underlying mechanism assumed in molecular kinetic theory (i.e. advancement of atoms from one adsorption site to another) is not present. If it is, though, the resistance force due to it is relatively small over the regime examined. It is possible forces related to interfacial friction become more pronounced once the droplet assumes a steady state advancing contact angle (i.e. $t \gtrsim 6$ ns); this is examined from a mechanistic point of view in what follows.

Continuum scale research methods often use fluid flow descriptions to compute flow velocity fields as a means of analyzing material transport in a liquid drop during spreading. An often discussed challenge for such numerical approaches are boundary conditions assumed, which are needed to permit numerical solution and avoid, for instance, singularities in the stress driving flow. Such flow fields can be calculated directly from atomic scale simulations where the contact line and other relevant boundaries are explicitly modeled. Figure 5 presents flow lines calculated from a simulation of Ag(l) on Ni(100) at $T = 1200$ K. Given the cylindrical geometry adopted, flow analysis is restricted to the xz plane. A regular grid of volume elements with size 0.5 nm $\times$ 0.5 nm (extending through the simulation cell in y) was defined. The (x, z) coordinates of atoms in each volume element were used at a given instant in time to compute the element's (x, z) center of mass position; this was repeated 0.6 ns later, providing the average displacement (and velocity) of material in each volume element over the considered time frame. The duration of time used was chosen to be long enough to provide reasonable statistics but short enough to offer good temporal resolution in the analyses. By plotting vectors corresponding to each element's average material velocity, a representation of flow in the nanometer scale spreading droplet is obtained.

Results in figure 5 show that analysis performed as described on an atomistic system modeled via MD does not give perfectly symmetric results as are typically obtained from continuum flow descriptions. This is a manifestation of the discrete, atomic nature to flow and wetting exhibited in MD simulations. Consider that data such as those shown in figure 5 are gathered by considering a sequence of non-equilibrium atomic coordinate sets corresponding to time progression. Starting from an initial condition of a drop in isothermal contact with a substrate, paths forward in time correspond with a sequence of spatial atomic ensembles. From a given starting atomic ensemble, the number of ensemble sequences that correspond with perfectly symmetric flow is very small compared to the number of sequences that correspond with asymmetric flow patterns. If this is interpreted as an entropy for non-equilibrium processes, the probability of a sequence of atomic ensembles showing perfect symmetry of flow for a nanometer scale droplet is very low. If multiple simulations were run, all for the same state point and geometry but with a different specific distribution of atomic coordinates and velocities at $t = 0$, and flow fields were calculated in each simulation and averaged together, it is expected that greater symmetry would emerge in flow fields so described. Similarly, when a macroscale drop is considered and analysis volume elements are defined with macroscale dimensions, significantly greater averaging occurs relative to the analysis illustrated in figure 5. As such, macroscale drops can be expected to exhibit greater symmetry of flow due to more significant volume averaging. Nonetheless, results such as those in figure 5 emphasize that, at the nanometer scale, the discreteness of matter at the atomic scale manifests in observed flow for a single droplet.

In the absence of averaging computed flow fields over multiple nanometer scale drop simulations, it is prudent to consider only qualitative features of flow during spreading. Given this constraint, some notable features can nonetheless be observed in figure 5, where larger vectors indicate more significant flow. Vectors near the top and center of the drop exhibit downward flow with velocity magnitude decreasing in time. At early time, flow into the edge of the drop occurs fairly uniformly from more central regions; this is illustrated by horizontal velocity vectors of comparable magnitude distributed across analysis volume elements extending in z from the solid/liquid interface, through the 'bulk' of the drop, to the liquid/vapor interface (see, for instance, flow lines within $\sim$25 nm of the drop edge in figures 5(a) and (b)). As time and spreading progress, features in the flow fields emerge indicative of stagnation regions near the solid/liquid interface. These are indicated by regions in which vectors are relatively small, indicating low flow velocity. Flow lines for material transport into the drop edge region are seen to bend around these areas of suppressed flow. In all cases observed, stagnation regions appear to have a size of approximately single digit nanometers; given this, the influence of such features on flow may only manifest for nanoscale droplets. However, if they exist with sufficient density near the contact line in macroscale droplets, they may collectively represent a form of solid/liquid friction as invoked, for instance, in molecular kinetic theory. Stagnation regions here may also be associated with observed deviations from $t^{1/2}$ kinetics in $R(t)$ data presented above. The origin of such regions is the zero flow velocity of atoms in the solid surface. Ag atoms in the drop adsorb to the solid/liquid interface and their interaction with solid Ni atoms is sufficient to constrain their motion. Such Ag atoms cannot be described as solidified yet they lack mobility typical of a liquid phase atom. This sort of transitional behavior, whether it be structural or dynamic, may be described as interphase. Here, interphase dynamic behavior of Ag(l) atoms results in regions of suppressed flow—stagnation regions—near the solid/liquid interface.

Flow into the droplet edge region appears fairly uniform throughout the simulation from data given in figure 5. Careful inspection of velocity vectors less than 5 nm from the contact line in x shows that, for grid elements more than $\sim$1 nm from the liquid/vapor interface, flow lines exhibit a

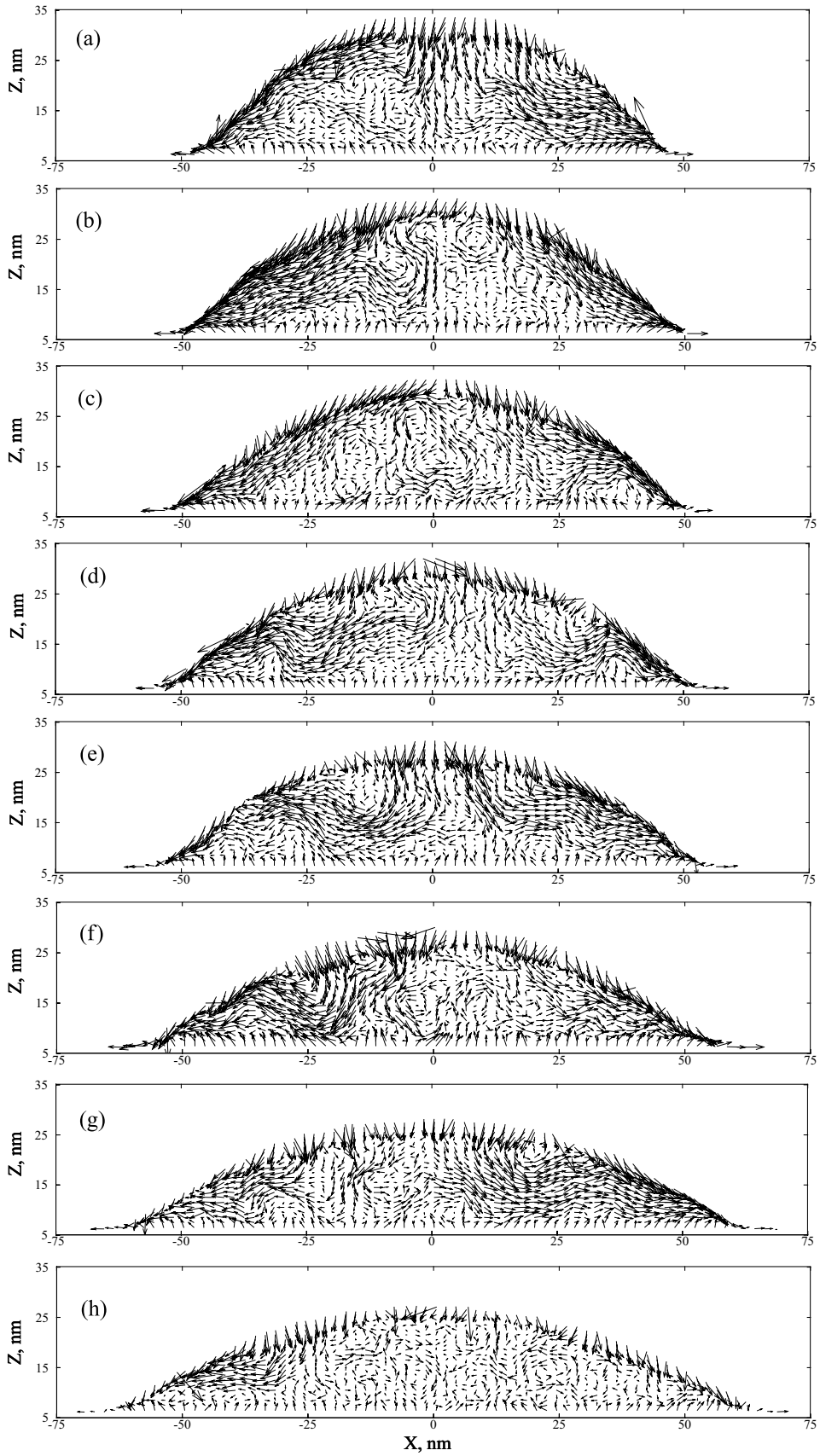

Figure 5. Velocity vectors of Ag(l) wetting on Ni(100) at $T = 1200$ K. Images from (a) to (h) are shown for $t = 3.0$–3.6, 3.6–4.2, 4.2–4.8, 4.8–5.4, 5.4–6.0, 7.0–7.6, 8.6–9.2, and 10.2–10.8 ns.

significant horizontal component. Velocity vectors for grid elements containing material within ∼1 nm of the liquid vapor interface are pointed along the liquid/vapor interface, directly at the contact line. This is suggestive of a mechanism by which transport along the liquid/vapor interface brings material preferentially to newly forming solid/liquid and liquid/vapor interface, at the contact line; at that position, liquid/vapor interface material converts to solid/liquid interface, deforming the liquid/vapor interface to cover greater area. Deformation of the liquid/vapor interface creates an analog to vacancies in the interface; liquid in more central regions of the drop away from the liquid/vapor interface flows predominantly in the spreading direction and, upon reaching the liquid/vapor interface fills vacancies. Such a mechanism implies that solid/liquid interface formed as the drop spreads arises predominantly from atoms that were previously at the liquid/vapor interface. This further implies that the mechanism of liquid atoms transferring between neighboring sites in the solid/liquid interface assumes a lesser role in the advancement of the contact line for simulations here.

MD simulations provide temporal and spatial resolution sufficient to probe fundamental flow and transport behavior postulated above. A qualitative example of the spatial and temporal resolution of MD is given in figure 6 where simulation snapshots show the evolution of Ag(l) atoms into the droplet edge; figure 6 also shows where atoms comprising the drop edge at a given moment are transported as the drop edge advances farther, creating new solid/liquid and liquid/vapor interfaces. The drop edge is defined in a fairly arbitrary way: all drop atoms less than 7 nm from the contact line in x at a given instant in time are said to be in the edge region; this definition corresponds to ∼25 atomic spacings along x. All Ag atoms in the edge region at $t = 4$ ns were identified; in all frames of figure 6, these atoms are colored light gray, other Ag atoms are darker gray and Ni atoms are black. Ensemble trajectories from MD permit one to track each of those atoms as a function of time, providing a description of material transport to the edge as well as a description of what happens to edge material as the drop spreads farther. Figure 6(a) at $t = 2$ ns shows that Ag atoms not yet in the edge region are distributed in z fairly uniformly. These atoms, though flowing towards the edge region, are far enough away from it in the drop that more rapid flow near the liquid/vapor interface is not apparent from material flow behavior. Figure 6(b) for $t = 3$ ns provides some indication that liquid/vapor interfacial flow may be influencing material flow into the edge region as so defined. Ag atoms which will enter the edge region over the following ns are somewhat concentrated in z closer to the liquid/vapor interface than the solid/liquid interface. This is related to a stagnation flow region near the solid/liquid interface as shown in figures 5(c) and (d), for instance, where the velocity vectors are small near the solid/liquid interfacial region. Atoms flowing into the edge must bend around stagnation regions (i.e. preferentially towards the liquid/vapor interface). Figures 6(d) and (e) for $t = 5$ and 6 ns show that, as the contact line advances, a significant portion of Ag atoms in our defined edge region at $t = 4$ ns, remain near the drop edge; they can also be seen to predominantly cluster near the solid/liquid interface. Liquid/vapor interface flow can be seen to bring new material into the edge region: note in figures 6(d) and (e) the growing region of dark gray moving from the drop into the edge region, along the liquid/vapor interface. Results such as those in figure 6 provide a qualitative description that Ag(l) atoms near the drop edge at a given instant experience a gradient in flow as the contact line advances and the solid/liquid and liquid/vapor interfaces grow. Flow into the contact line is preferentially from along the liquid/vapor interface; accordingly, flow into the region near the drop edge is preferentially more rapid near the liquid/vapor interface. This flow effectively spreads out edge material over the solid/liquid interface.

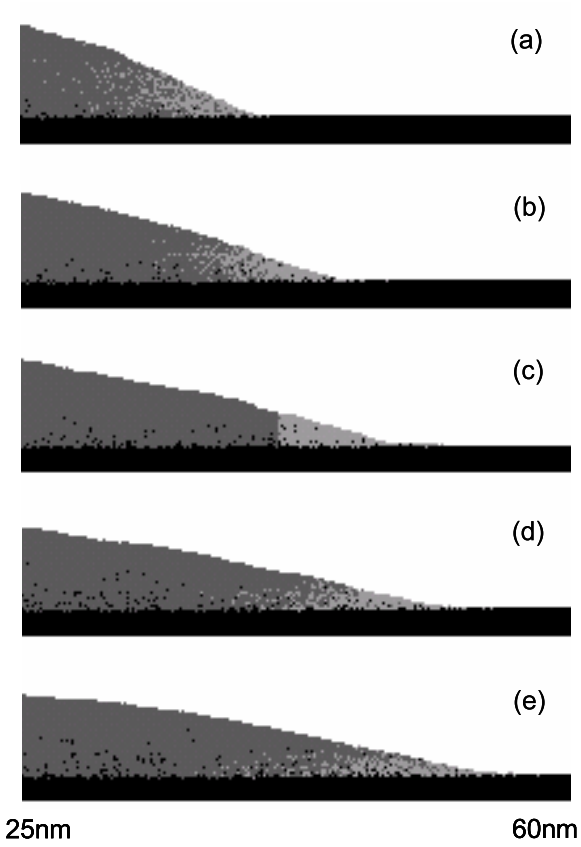

Figure 6. Transport history of Ag atoms present in the contact line region (in light gray) at $t = 4$ ns for Ni(100). Images from (a) to (e) are shown for $t = 2$, 3, 4, 5, and 6 ns. Ag atoms not in the contact line region at $t = 4$ ns are dark gray and Ni atoms are black.

A quantitative illustration of atomic transport characteristics near the contact line can be obtained from atomic positions as a function of time. Specifically, statistics for atom position history can be compared for atoms in the drop edge region and atoms in a similar volume element but away from the drop edge (i.e. near the drop center). Figure 7 shows such an analysis to explore the history of Ag(l) atoms forming the solid/liquid interface: the top panel shows the analysis for atoms near the drop center and the bottom panel is for atoms near the drop edge. Similar to the procedure for figure 6, all atoms within 7 nm of the contact line in x were identified at $t = 4$ ns; in this case though, only those edge atoms that were also in the first layer ($l = 1$) above the solid/liquid interface were selected.

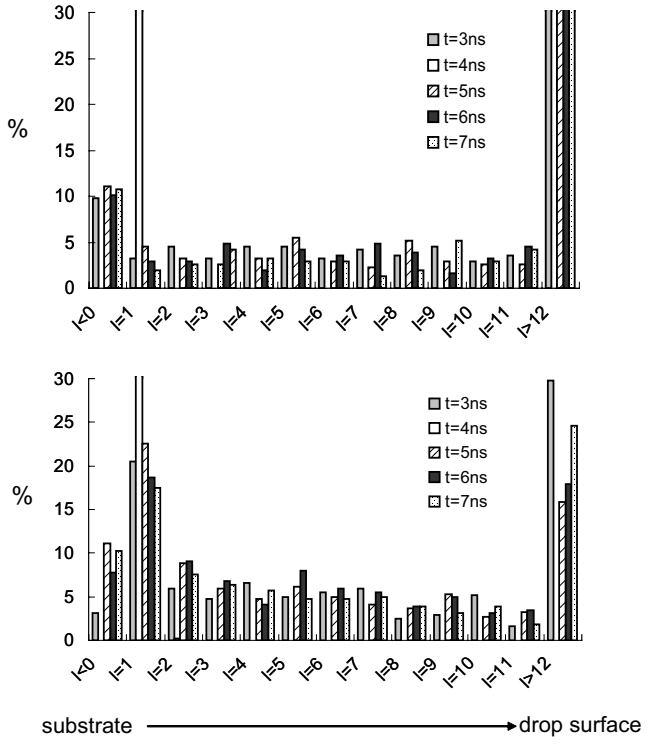

Figure 7. Height distribution for atoms at the first layer above the initial substrate surface within 7 nm of the drop center (top) and contact line (bottom) at $t = 3$, 4, 5, 6, and 7 ns.

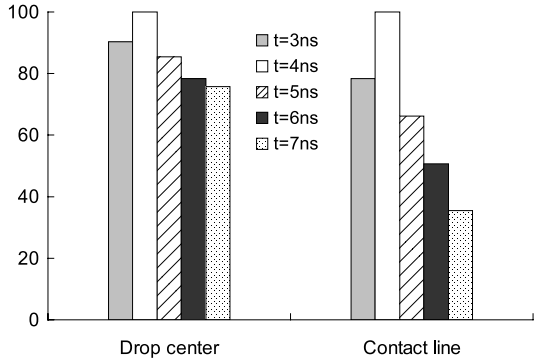

Figure 8. Percentage of Ag(l) atoms within 7 nm (in the x-direction) of the drop center (left) and contact line (right) at $t = 4$ ns, which remain within 7 nm of the drop center (left) and contact line (right) at $t = 3$, 5, 6, and 7 ns.

In other words, those atoms forming the solid/liquid interface in the drop edge region were identified. A similar sized population of atoms occupying the $l = 1$ layer but near the drop center were also identified. Given these two groups of atoms, their height in z above the solid/liquid interface was tracked as a function of time leading up to $t = 4$ ns and also beyond; results, in the form of probability for an atom in a selected group to occupy layers $l = -1$ to $l \geqslant 12$, are shown for the drop center (top panel) and drop edge (bottom panel) in figure 7. This results in a histogram of probabilities for each layer l, for each time analyzed $t = 3$, 4, 5, 6, and 7 ns. By definition, 100% of atoms analyzed in figure 7 are in the $l = 1$ layer at $t = 4$ ns; thus, the histogram for $t = 4$ ns is a single line plot with 100% at $l = 1$. Note that data for $l \geqslant 12$ represent atoms that were farther than ∼2.4 nm in z from the solid/liquid interface at the given time analyzed.

Figure 7 provides a quantitative description of the likelihood of atoms to remain near the solid/liquid interface if they are near the droplet edge versus in the droplet bulk. A different atomic position analysis is shown in figure 8 where data are presented to examine the probability that an atom near the edge of the drop remains near the edge of the drop (i.e. advances with the contact line). As was done to generate figure 6, all atoms less than 7 nm from the contact line in x (regardless of z) were identified at $t = 4$ ns. The percentage of those atoms that are also less than 7 nm from the contact line (in x) is calculated at $t = 3$, 5, 6, and 7 ns. A similar size population of atoms was selected for analysis near the drop center. To identify those latter atoms, drop atoms were counted with x coordinate less than 7 nm from the drop center. Atoms satisfying this constraint were sorted in z and selected starting with those at the solid/liquid interface; additional atoms with increasing z coordinate were included until the size of the analysis set was the same as that used for edge analysis. Symmetry demands that flow in the x direction should be near zero at the center of the drop and flow fields presented in figure 5 show this holds for simulations here. Given this, in the probability analysis of figure 8, data for the drop center should be predominantly determined by atomic diffusive transport in the liquid.

The histogram of probabilities in figure 8 for the drop center shows that the majority of atoms identified at $t = 4$ ns remain in the x bounds of the analysis region at subsequent time but that there is a gradual decrease in their numbers with time. We associate this behavior with diffusive transport of atoms away from this region of low flow. Results for atoms near the drop edge are quite different with a much more rapid decrease with time in the probability that an atom remains near the edge. Results in figure 8 show that, as new material is delivered into the drop edge region, associated flow preferentially drives material that was near the drop edge at one point in time away from the edge subsequently. Combining this observation with what was seen in figure 7, it can be argued that flow of material into the drop edge along the liquid/vapor interface effectively spreads existing edge material out along the solid/liquid interface as the contact line advances. One effect of this is to preferentially constrain existing edge material near the solid/liquid interface (figure 7). A perhaps more dominant effect illustrated in figure 8 is that this flow mechanism preferentially drives what was edge material to be left behind the advancing contact line. Note that figure 8 is based on a moving frame of reference for the analysis region at the drop edge; as such, if an atom is identified as not being in the analysis region, it must be behind it, relative to the contact line advancement direction. An analogy arises of a knife smearing a viscous liquid onto a surface where material that at one moment is deposited at the newly formed solid/liquid interface, is subsequently left behind as new material is advanced over top of it and down onto the growing interface at the contact line. In the case presented here, the push of a knife is replaced by the pull of capillarity. This

also imparts a notion of a form of rolling motion very local to the advancing contact line.

We have alluded numerous times to a dominance of transport along the liquid/vapor interface in determining contact line advancement for the system studied here. To quantitatively illustrate this, we analyze atomic transport into a relatively small volume element encompassing the contact line. In this analysis, the contact line region is defined in a frame of reference that moves with the contact line in x, $(R(t) - 0.2)$ nm $< x < (R(t) + 0.2)$ nm; in z, the contact line region is defined as consisting of atoms in layers 1 and 2. As in all our analyses, we average over the periodic drop thickness in y. This means the contact line region in x and z is of order one or two atomic sizes. At $t = 4$ ns, we find all atoms that are within 0.4 nm of the liquid/vapor interface; these atoms are sorted according to their distance away from (or behind) the contact line region and only those less than 4 nm behind the contact line were kept for analysis. Only atoms with x coordinate lower than the contact line region were considered to exclude the precursor film; thus, they were behind the contact line, relative to the spreading direction. Similarly, all atoms behind the contact line and in layers $l = 2$ and 3 were identified and sorted, keeping only those atoms less than 4 nm from the contact line. The first group of atoms were labeled liquid/vapor interface atoms and the latter were solid/liquid interface atoms. For these two groups, the percentage of atoms that subsequently entered the narrowly defined contact line region was computed as a function of time.

Figure 9 shows curves so obtained along with a graphical representation of the atoms in each analysis group. For both groups of atoms, a rapid increase in this percentage with time is initially observed, followed by a plateau. For liquid/vapor interface atoms, the rate of initial rapid increase is greater as is the plateau magnitude, compared to solid/liquid interface atoms. This is clear evidence of the preponderance of transport along the liquid/vapor interface in determining contact line advancement for this system. However, figure 9 also illustrates that mechanisms more commonly associated with molecular kinetic theory act here as well. Nearly 60% of solid/liquid interface atoms eventually move to the contact line, indicative of atoms detaching and re-attaching at solid/liquid interface adsorption sites. Comparing this to the nearly 85% probability for a liquid/vapor interface atom to reach the contact line shows liquid/vapor interface transport processes dominate contact line advancement—but only marginally so—over solid/liquid interface processes.

As a final illustration of the level of detail obtainable from MD simulations of high temperature contact line advancement, figure 10 presents illustrations of specific atomic trajectories near the contact line as it advances. While the power of simulations is to form statistical descriptions of many such trajectories, observing individual examples provides a flavor of the atomic scale mechanisms at work. Six atoms were randomly selected that were less than 0.5 nm from the contact line in both x and z at $t = 4$ ns (these atoms are within a single analysis element used in velocity vector calculations of figure 5); essentially, these atoms can be said to be at the contact line at $t = 4$ ns. Their trajectories in x and z are then

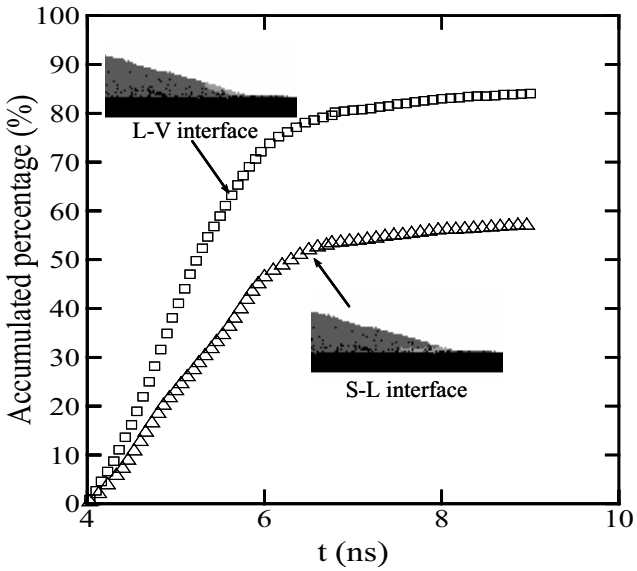

Figure 9. Accumulated possibility of liquid/vapor interfacial atoms (0.4 nm from the liquid/vapor interface and 0.2–4 nm to the contact line) versus solid/liquid interfacial atoms (Ag atoms in layers 2 and 3 above the substrate and 0.2–4 nm to the contact line) at 4 ns moving to the contact line region (±0.2 nm to the contact line in x, within 0.2 nm above substrate in z) in the next 5 ns.

plotted for 2 ns out to $t = 6$ ns. The x position of the contact line is plotted with a dark curve in each example. A collection of behaviors is exhibited. For instance, figure 10(a) shows an atom that, for the bulk of the 2 ns of analysis remains very near the contact line. This is a nearly ideal example of the sort of motion envisioned in the molecular kinetic model of spreading as the atom depicted moves along the solid/liquid interface in step with the contact line. This is also somewhat true for the trajectory in figure 10(b) where the atom generally advances in x with the contact line and remains near the solid/liquid interface for portions of the trajectory. Figures 10(c)–(e) show examples where the x position of the atom does not change dramatically; that is, it is left behind the contact line. In figures 10(c) and (e), the atom progresses away from the solid/liquid interface but returns to it; in figure 10(d) the atom falls behind the contact line but remains near the solid/liquid interface. Finally, in figure 10(f) the atom is seen to move opposite the flow direction in x; nonetheless, it does not, for the duration analyzed, move more than 10 nm from the solid/liquid interface. These are simply example trajectories and greater benefit is found in more collective analyses. Nonetheless, results in figure 10 along with those presented throughout, illustrate the myriad atomic behavior responsible for contact line advancement in this high temperature capillary system.

It is important to note that the size of the droplet examined in this study is at the nanometer scale (i.e., $R = 25$ nm) and that observations for this length scale droplet may not extend to macroscale droplets. Indeed, an outstanding question is whether fundamentally different physical phenomena of wetting exist for very small droplets compared to droplets observed via experiments or continuum calculations and, if size effects exist, at what length scale do they emerge.

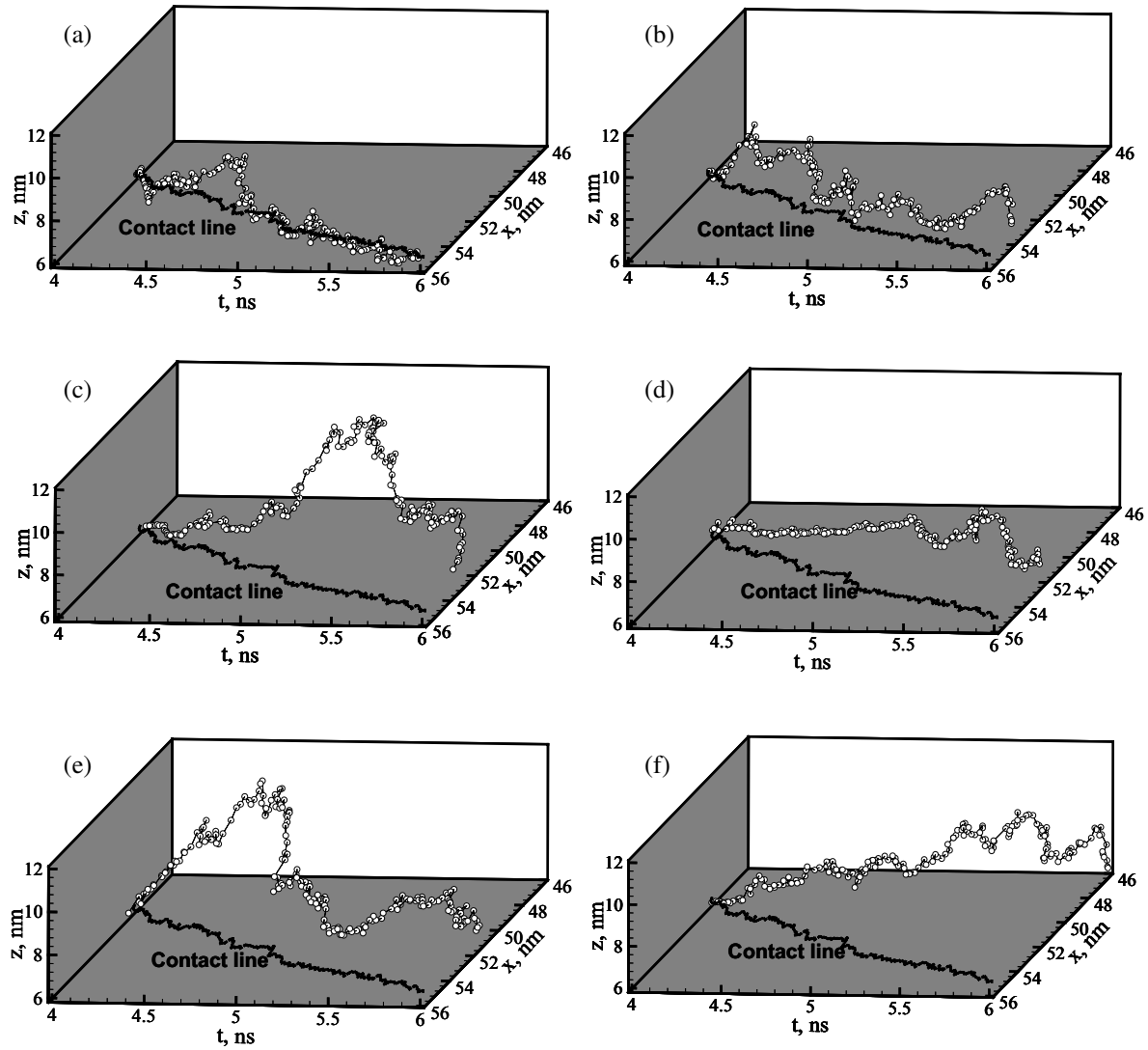

Figure 10. Atomic trajectories in x and z from $t = 4$ to 6 ns for six different atoms, all of which were within 0.5 nm of the contact line at $t = 4$ ns. A solid line in the $z = 0$ plane shows the position in x of the contact line over the same time period.

Nonetheless, it is reasonable to expect that fluid flow inside the bulk of the droplet is affected by the confined drop dimension. A less obvious question is whether mechanisms of material transport local to the contact line differ for a nanometer scale droplet compared to macroscale droplets. If 'local to the contact line' is defined as within 5–10 nm, it seems likely that mechanisms observed herein manifest in macroscale droplets as well. This is important because results such as those presented here may provide a means of constructing new boundary conditions for contact line behavior in continuum models and theory; parameters for such models may then be calculated from atomic scale simulations. For instance, an atomic transport mechanism of contact line motion demonstrate here asserts that new material from the bulk of the droplet is brought into the contact line close to the liquid/vapor interface; furthermore, this mechanism preferentially causes material at the contact line at one instant in time to be left behind (near the solid/liquid interface) as the contact line advances. Such a mechanism is akin to the 'rolling effect' observed in a macroscopic drop wetting experiment [19], or the 'tank tread' motion of the liquid molecules normal to the solid substrate [42]. It can be argued that, once the contact line wedge is formed, this rolling motion in the vicinity of the contact line is a local effect that exists regardless of the overall droplet size. However, a remaining exercise is to evaluate mechanisms of contact line advancement local to the contact line as droplet size is increased from the present nanoscale drop wetting simulations to increasingly larger droplets. An additional remaining exercise is to evaluate the degree to which liquid/vapor transport influences contact line advancement in other systems. This may be a feature unique to very high velocity spreading systems; perhaps related to this, it may only emerge for metal liquids with relatively low surface tensions.

5. Conclusions

MD simulations of Ag(l) wetting Ni substrates were used to examine atomic mechanisms of flow associated with contact line advancement. A case was selected where dissolution of

the substrate was relatively slow and wetting kinetics were predominantly dictated by capillary forces. Results indicate that material is preferentially delivered to the advancing contact line along the liquid/vapor interface. As this interface grows, material from within the drop flows predominantly parallel to the spreading direction until it reaches the liquid/vapor interface. Flow of new material into the drop edge along the liquid/vapor interface spreads existing edge material along the solid/liquid interface; this creates a flow pattern that preferentially leaves what was once edge material behind the advancing contact line. Despite the presence of this liquid/vapor interface flow, evidence is still found for a mechanism of contact line advancement described by molecular kinetic theory. Some portion of atoms that form the solid/liquid interface near the contact line move along with the contact line, desorbing and re-adsorbing between neighboring solid/liquid interface sites. Results such as those presented here bear out the complex interplay of mechanisms that may underlie wetting and spreading behavior at high temperature. They also emphasize the utility of using simulation methods such as MD to study capillary phenomena, particularly from a mechanistic point of view.

Acknowledgments

This work was supported in part by the National Science Foundation under Grant No. DMR-0606408. Sandia is a multiprogram laboratory operated by Sandia Corporation, a Lockheed Martin Company, for the United States Department of Energy's National Nuclear Security Administration under contract DE-AC04-94AL85000.

References

[1] Boyer H E and Gall T L 1985 *Metals Handbook* Desk edn (Metals Park, OH: American Society of Metals)
[2] Wassink R J K 1989 *Soldering in Electronics* (British Isles: Electrochemical Publications)
[3] Otten A and Herminghaus S 2004 *Langmuir* **20** 2405
[4] Sharps P R, Tomsia A P and Pask J A 1981 *Acta Metall.* **29** 855
[5] Yin L, Murray B T and Singler T J 2006 *Acta Mater.* **54** 3561
[6] Landry K and Eustathopoulos N 1996 *Acta Mater.* **44** 3923
[7] Huh C and Scriven L 1971 *J. Colloid Interface Sci.* **35** 85
[8] Tanner L H 1979 *J. Phys. D: Appl. Phys.* **12** 1473
[9] Blake T D and Haynes J M 1969 *J. Colloid Interface Sci.* **30** 421
[10] Cherry B W and Holmes C M 1969 *J. Colloid Interface Sci.* **29** 174
[11] Mortensen A, Drevet B and Eustathopoulos N 1997 *Scr. Mater.* **36** 645
[12] Warren J A, Boettinger W J and Roosen A R 1998 *Acta Mater.* **46** 3247
[13] Webb E B III, Grest G S, Heine D R and Hoyt J J 2005 *Acta Mater.* **53** 3163
[14] de Gennes P G 1985 *C.R. Acad. Sci., Paris* **300** 839
[15] Abraham D B, Collet P, de Coninck J and Dunlop F 1990 *Phys. Rev. Lett.* **65** 195
[16] Yang J, Koplik J and Banavar J R 1991 *Phys. Rev. Lett.* **67** 3539
[17] Moon J, Yoon J, Wybblatt P, Garoff S and Suter R M 2002 *Comput. Mater. Sci.* **25** 503
[18] Webb E B III, Grest G S, Heine D R and Hoyt J J 2003 *Phys. Rev. Lett.* **91** 236102
[19] DussanV E B and Davis S H 1974 *J. Fluid Mech.* **65** 71
[20] Saiz E, Tomsia A P, Rauch N, Scheu C, Ruehle M, Benhassine M, Seveno D and de Coninck J 2007 *Phys. Rev.* E **76** 041602
[21] Saiz E and Tomsia A P 2004 *Nat. Mater.* **3** 903
[22] Allen M and Tildesley D 1987 *Computer Simulation of Liquids* (New York: Oxford University Press)
[23] Webb E B III, Hoyt J J and Grest G S 2005 *Curr. Opin. Solid State Mater. Sci.* **9** 174
[24] De Coninck J and Blake T D 2008 *Annu. Rev. Mater. Res.* **38** 1
[25] Prévot G, Cohen C, Guigner J M and Schmaus D 2000 *Phys. Rev.* B **61** 10393
[26] Moon J, Lowekamp J, Wybblatt P, Garoff S and Suter R M 2001 *Surf. Sci.* **488** 73
[27] Prévot G, Cohen C, Schmaus D and Pontikis V 2000 *Surf. Sci.* **459** 57
[28] Prévot G, Cohen C, Moulin J and Schmaus D 1999 *Surf. Sci.* **421** 364
[29] Kellogg G L and Plass R A 2000 *Surf. Rev. Lett.* **7** 649
[30] Webb E B III and Hoyt J J 2008 *Acta Mater.* **56** 1802
[31] Milner D R 1958 *Br. Weld. J.* **3** 90
[32] Daw M S and Baskes M I 1984 *Phys. Rev.* B **29** 6443
[33] Foiles S M, Baskes M I and Daw M S 1986 *Phys. Rev.* B **33** 7983
[34] Singleton M and Nash P 1987 *Bull. Alloy Phase Diagr.* **8** 119
[35] Hoyt J J, Garvin J W, Webb E B III and Asta M 2003 *Modelling Simul. Mater. Sci. Eng.* **11** 287
[36] Foiles S M and Adams J B 1989 *Phys. Rev.* B **40** 5909
[37] Plimpton S J 1995 *J. Comput. Phys.* **117** 1
[38] Lopez J, Miller C A and Ruchenstein E 1976 *J. Colloid Interface Sci.* **56** 460
[39] Heine D R, Grest G S and Webb E B III 2004 *Phys. Rev.* E **70** 011606
[40] Webb E B III and Grest G S 2001 *Phys. Rev. Lett.* **86** 2066
[41] Blake T D, Clarke A, Coninck J D, de Ruijter M and Vou'e M 1999 *Colloids Surf.* A **149** 123
[42] Hoffman R L 1983 *J. Colloid Interface Sci.* **94** 470